On the Symbol Error Rates for Signal Space Diversity Schemes over a Rician Fading Channel

Jihoon Kim, Wonjun Lee, Jong-Kook Kim, and Inkyu Lee

***Abstract*—A signal space diversity (SSD) scheme is one of techniques to achieve diversity gain in fading channels. This method consists of two key operations: constellation rotation and component-wise interleaving. Because of these operations, the decision boundaries for the SSD are no longer perpendicular, and thus, different coordination approaches are required for the analysis of error rates compared to conventional rectangular coordinates. In this letter, we derive an exact expression of the symbol error rate for the SSD scheme in Rician fading channels with M-QAM and M-PSK. By defining the ratio of the standard deviation of the inphase and quadrature components, we introduce a new signal model for the SSD. Based on this signal model, we can compute the exact symbol error rate using polar coordinates. The computer simulation results confirm the accuracy of our analysis for fading channels.**

***Index Terms*—Signal space diversity (SSD), Rician fading channels, polar coordinates, symbol error rates (SER).**

I. Introduction

DIVERSITY is an effective means to combat fadings in wireless communication systems. When several replicas of the same information are available, a receiver combines them to increase the received signal-to-noise ratio (SNR) to improve the system performance [1]. Moreover, if each replica experiences uncorrelated fadings, diversity order can be increased. Signal space diversity (SSD) has been introduced as an alternative scheme to achieve an additional diversity gain in single antenna systems [2]. The SSD involves interleaving over coordinates and employs signal constellation rotation. The diversity can be increased to the minimum number of distinct coordinates associated with an error event by optimally rotating the constellation and separately interleaving the signals in each coordinate. As the signal experiences independent fading effects, the SSD shows a significant performance improvement over conventional systems. In general, it is possible to employ the SSD in a N complex dimension in order to achieve a diversity order of N.

Exact evaluation of an error rate is one of the fundamental problems for the system design. Many studies have been reported for evaluating the error rate in various approaches [3] [4]. The error rate computation is generally carried out using rectangular coordinates for conventional M-QAM constellations. However, since the SSD technique employs component-wise interleaving and constellation rotation, decision boundaries for the SSD are not perpendicular even for M-QAM constellations. The union bound based on the pair-wise error probability (PEP) under Rayleigh fading channels was derived for the SSD [5] [6] [7]. However, the analytical results in [5] still show a 0.7dB gap from the actual simulation for 16-QAM. Recently, a tight lower bound for rotated lattice constellations in general fading channels is reported in [8].

In this letter, we derive an exact expression for the error performance of the SSD technique over Rician fadings using polar coordinates as introduced in [9] and [10]. Here, we focus on the two dimensional SSD, which is normally implemented by employing the inphase and the quadrature interleaving independently. To this end, we first develop a new channel model for the SSD, and determine decision regions for each symbol for the given constellation. Then, we calculate the probability of correct decisions for each region by applying distributions of the magnitude and the phase of the noise. Based on these probabilities, we evaluate an exact expression of the error rate for M-QAM and M-PSK in Rician channels. The simulation results confirm the accuracy of our analysis.

The organization of this letter is as follows. In Section II, we review the signal model for the SSD scheme briefly. In Section III, we show the evaluation of the symbol error rate (SER) for the SSD using the polar coordinates in detail. Section IV exhibits the numerical results to verify our derivation. Finally, the conclusion is given in Section V.

II. Signal Model

In this letter, we consider a communication system employing the SSD scheme with component interleaving over fading channels. We assume that there is no intersymbol interference (ISI) and any other impairments except additive noise. Here we define $s[i]$ and $x[i]$ as the ith signal sample from a given constellation $\mathcal{X} = \{s_0, \cdots, s_{M-1}\}$ and the ith transmitted signal sample after the component interleaving, respectively. Note that $\mathcal{X}$ is a rotated constellation with the rotation angle θ_R.

Let us denote the subscripts I and Q as the inphase and quadrature components, respectively. In the SSD system, the inphase and quadrature components $\{s_I[i]\}$ and $\{s_Q[i]\}$ go through two independent interleavers and are transformed to $\{x_I[i]\}$ and $\{x_Q[i]\}$. In other words, each $s[i]$ is transmitted at different time, and thus experiences different fadings. Then,

Paper approved by M.-S. Alouini, the Editor for Modulation and Diversity Systems of the IEEE Communications Society. Manuscript received October 26, 2007; revised June 2, 2008 and October 13, 2008.

J. Kim, J.-K. Kim, and I. Lee are with the School of Electrical Engineering, Korea University, Seoul Korea (e-mail jihoon@wireless.korea.ac.kr; {jongkook, inkyu}@korea.ac.kr).

W. Lee is with the Division of Computer and Communication Engineering, Korea University, Seoul Korea (e-mail: wlee@korea.ac.kr).

This work was presented in part at the 2008 IEEE International Conference on Communications (ICC'08), Beijing, May 2008. This work was supported by the MKE (Ministry of Knowledge Economy), Korea, under the ITRC (Information Technology Research Center) support program supervised by the IITA (Institute for Information Technology Advancement) (IITA-2008-C1090-0801-0013).

Digital Object Identifier 10.1109/TCOMM.2009.08.070148

the ith received signal sample $r[i]$ is given by

$$r[i] = h[i]x[i] + w[i],$$

where $h[i]$ represents the complex fading coefficient and $w[i]$ indicates the additive noise. Here we assume that $h[i]$ has a Rician distribution with unit variance ($E[|h[i]|^2] = 1$) and $w[i]$ has a Gaussian distribution with zero mean and variance N_0 ($E\left[|w[i]|^2\right] = N_0$).

It is assumed that channel state information (CSI) is available at the receiver side. To detect $s[i]$, the received signal is divided by the corresponding channel coefficient $h[i]$ as $y[i] \triangleq r[i]/h[i] = x[i] + \mu[i]$ where $\mu[i] = w[i]/h[i]$. Then, $y[i]$'s are component-wise deinterleaved to estimate the transmitted symbol $s[i]$. Defining n and m as the indices corresponding to index i of the inphase and the quadrature components after deinterleaving, respectively, the deinterleaved signal sample at the ith time, denoted by $z[i]$, is obtained as

$$\begin{aligned} z[i] &= y_I[n] + jy_Q[m] \\ &= (x_I[n] + \mu_I[n]) + j\,(x_Q[m] + \mu_Q[m]) \\ &= x_I[n] + jx_Q[m] + \mu_I[n] + j\mu_Q[m] \\ &= s[i] + \nu[i] \end{aligned} \tag{1}$$

where $j = \sqrt{-1}$ and we define $\nu[i] = \mu_I[n] + j\mu_Q[m]$ as the noise sample of $z[i]$.

In (1), the inphase and quadrature parts of the noise $\nu[i]$ have statistically independent Gaussian distributions with different variances due to component-wise deinterleaving. Based on (1), the maximum likelihood (ML) detector decides the estimated symbol $\hat{s}[i]$ as

$$\begin{aligned} \hat{s}[i] &= \arg\max_{s[i]\in\mathcal{X}} \left\{ \exp\left(-\frac{|z_I[i] - s_I[i]|^2}{\sigma_I^2} - \frac{|z_Q[i] - s_Q[i]|^2}{\sigma_Q^2} \right) \right\} \\ &= \arg\min_{s[i]\in\mathcal{X}} \left(\frac{|z_I[i] - s_I[i]|^2}{\sigma_I^2} + \frac{|z_Q[i] - s_Q[i]|^2}{\sigma_Q^2} \right) \\ &= \arg\min_{s[i]\in\mathcal{X}} \left(|z_I[i] - s_I[i]|^2 + R^2 |z_Q[i] - s_Q[i]|^2 \right) \end{aligned} \tag{2}$$

where σ_I^2 and σ_Q^2 denote the variances of the inphase part and quadrature part of $\nu[i]$, respectively, and we define $R = \sigma_I/\sigma_Q$ as the ratio of the standard deviation of the inphase and quadrature parts. We omit the index i for the rest of this letter for simplicity.

Now we want to modify (1) to simplify the analysis. We introduce a new signal model as

$$\begin{aligned} \bar{z} &= z_I + jR \cdot z_Q \\ &= s_I + jR \cdot s_Q + n_I + jR \cdot n_Q \\ &\triangleq \bar{s} + \bar{\nu} \end{aligned} \tag{3}$$

where $\bar{s}$ and $\bar{\nu}$ represent the transmitted data and the noise in the new signal model, respectively.

Observing that the quadrature part of $\bar{\nu}$ is still Gaussian and its variance is equal to that of the inphase part, denoted by $A \triangleq E[\nu_I^2] = \sigma_I^2$, this result indicates that the new signal model (3) is equivalent to the conventional additive white Gaussian noise (AWGN) model with $E[|\bar{\nu}|^2] = 2A$. Therefore, the ML decision metric for the new signal model (3) can simply be written as

$$\hat{s} = \arg\min_{\bar{s}\in\bar{\mathcal{X}}} |\bar{z} - \bar{s}|^2 \tag{4}$$

where $\bar{\mathcal{X}} = \{\bar{s}_k = s_{k,I} + jR \cdot s_{k,Q}, k = 0, \cdots, M-1\}$ denotes the new constellation obtained by scaling the quadrature part of the original constellation $\mathcal{X}$ by R as in (3). Note that this simple metric (4) is equivalent to the original metric (2).

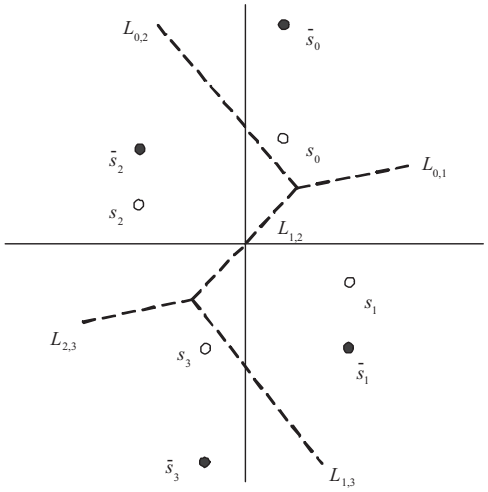

Fig. 1. New 4-QAM constellation $\bar{\mathcal{X}}$ and its decision region for $R > 1$.

For this new constellation $\bar{\mathcal{X}}$, we define the decision boundary between $\bar{s}_k$ and $\bar{s}_p$, denoted by $L_{k,p}$, as

$$\begin{aligned} L_{k,p} &= \left\{ \bar{z} : |\bar{z} - \bar{s}_k|^2 = |\bar{z} - \bar{s}_p|^2 \right\} \\ &= \{(\bar{z}_I, \bar{z}_Q) : 2(s_{p,I} - s_{k,I})\bar{z}_I + 2R(s_{p,Q} - s_{k,Q})\bar{z}_Q \\ &\quad -(s_{p,I}^2 + R^2 s_{p,Q}) + (s_{k,I}^2 + R^2 s_{k,Q}) = 0\}. \end{aligned} \tag{5}$$

Thus, the decision region for $\bar{s}_k$ is formed as a convex polygon surrounding the symbol. For example, Figure 1 shows the rotated 4-QAM constellation $\mathcal{X}$ (empty circle) and the new constellation $\bar{\mathcal{X}}$ (filled circle) for $R > 1$. Also, we depict decision boundaries of the new constellation as the dashed line in this figure. Note that the decision boundaries of $\bar{\mathcal{X}}$ are not perpendicular, while those of $\mathcal{X}$ are. Notice that the decision regions of $\bar{\mathcal{X}}$ change according to R. For given R, we can find the polygon's sides efficiently using the method proposed in [11].

III. Evaluation of SER for SSD

In this section, we derive the SER expression of the SSD system for M-QAM and M-PSK constellation.

A. Error Rates for 4-QAM and 16-QAM Constellation

In order to evaluate the error rate, we first calculate the probability of correct decisions for each symbol $\bar{s}_k$ given R and A, denoted by $P_c(R, A|\bar{s}_k)$, which can be expressed in terms of the noise distribution [12]. For conventional systems with perpendicular decision boundaries, the error probability for M-QAM constellations is obtained as the product of the Q-function in rectangular coordinates. However, for the SSD, the decision regions are no longer identical for each symbol

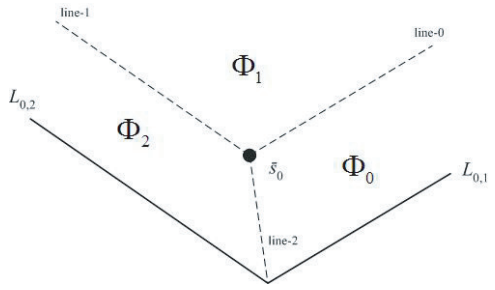

Fig. 2. Separations of the decision region for $\bar{s}_0$ in new 4-QAM constellation ($R > 1$).

as shown in Figure 1. For this reason, in order to evaluate the exact error probability, we employ polar coordinates instead of rectangular coordinates.

Denote $\bar{\nu}_M$ and $\bar{\nu}_\phi$ as the magnitude and the angle of $\bar{\nu}$ in (3), respectively. Then, $\bar{\nu}_M$ has a Rayleigh distribution with $E\left[\bar{\nu}_M^2\right] = 2A$, and $\bar{\nu}_\phi$ is uniformly distributed. The probability density function (pdf) of $\bar{\nu}$ is given as

$$p(\bar{\nu}) = \frac{1}{2\pi}\frac{\bar{\nu}_M}{A}\exp\Big(-\frac{\bar{\nu}_M^2}{2A}\Big).$$

Thus, correct decisions are made if the sum of the transmitted symbol and the noise with the above distribution remains within the decision region.

Let us define $d(\phi)$ as the distance from a symbol to the decision boundary which has an angle $\phi \in \Phi = [\phi_1, \phi_2]$ with respect to the x-axis. Then, we can express the probability of correct decisions by integrating the pdf of the noise as

$$\begin{aligned} P_c &= \int_{\phi_1}^{\phi_2}\int_0^{d(\phi)} \frac{1}{2\pi}\frac{\bar{\nu}_M}{A}\exp\Big(-\frac{\bar{\nu}_M^2}{2A}\Big)d\bar{\nu}_M d\phi \\ &= \frac{1}{2\pi}(\phi_2-\phi_1) - \frac{1}{2\pi}\int_{\phi_1}^{\phi_2}\exp\left(-\frac{d^2(\phi)}{2A}\right)d\phi. \quad (6) \end{aligned}$$

Next, we define the following notations as

- $l(a,b)$: the line which connects two points a and b
- $\theta(l)$: the angle of the line l with respect to the x-axis ($\theta(l) \in [0,\pi]$)
- $d_{k,p}$: the half distance between $\bar{s}_k$ and $\bar{s}_p$
- $\bar{z}(k,p,q)$: the intersection point between boundaries $L_{k,p}$ and $L_{k,q}$.

First we consider the decision region for $\bar{s}_0$ in 4-QAM constellation shown in Figure 2. In this case, the decision region for $\bar{s}_0$ can be divided into three subregions by three lines which are labeled as line-0, line-1 and line-2 in Figure 2. The line-0 and line-1 are drawn parallel to $L_{0,1}$ and $L_{0,2}$, respectively. The intersection point $\bar{z}(0,1,2)$ can be obtained by solving $L_{0,1} - L_{0,2} = 0$ in (5).

Therefore, we can express each subregion in terms of the range of the angle: $\Phi_0 = [\theta(l(\bar{s}_0, \bar{z}(0,1,2))) - \pi, \theta(L_{0,1})]$, $\Phi_1 = [\theta(L_{0,1}), \theta(L_{0,2})]$ and $\Phi_2 = [\theta(L_{0,2}), \theta(l(\bar{s}_0, \bar{z}(0,1,2))) + \pi]$. For a given angle ϕ in the subregion Φ_0, the magnitude of the noise should be less than $d(\phi) = \frac{d_{0,1}}{\cos(\pi/2 - \theta(L_{0,1}) + \phi)}$ to make correct decisions. Similarly, for the subregion Φ_2, the magnitude of the noise for correct decisions is given by $d(\phi) = \frac{d_{0,2}}{\cos(\pi/2 + \theta(L_{0,2}) - \phi)}$. Unlike these subregions, there is no limit on the magnitude of the noise for the subregion Φ_1. In other words, no error will be made regardless of the magnitude of the noise in this subregion. By combining the above results, the probability of correct decisions for $\bar{s}_0$ can be obtained as

$$\begin{aligned} &P_c(R, A|\bar{s}_0) \\ &= 1 - \frac{1}{2\pi}\int_{\Phi_0}\exp\left(-\frac{d_{0,1}^2}{2A\sin^2(\theta(L_{0,1}) - \phi)}\right)d\phi \\ &\quad - \frac{1}{2\pi}\int_{\Phi_2}\exp\left(-\frac{d_{0,2}^2}{2A\sin^2(\theta(L_{0,2}) - \phi)}\right)d\phi \\ &= 1 - \xi(A, d_{0,1}, \theta(L_{0,1}), \Phi_0) - \xi(A, d_{0,2}, \theta(L_{0,2}), \Phi_2) \end{aligned}$$

where we define $\xi(A, d, \theta, \Phi)$ as

$$\xi(A, d, \theta, \Phi) = \frac{1}{2\pi}\int_{\Phi}\exp\left(-\frac{d^2}{2A\sin^2(\theta - \phi)}\right)d\phi.$$

Using a similar approach, we can calculate $P_c(R, A|\bar{s}_1)$ for the symbol $\bar{s}_1$ in Figure 1. The decision region for $\bar{s}_1$ can be separated by four subregions: $\Phi_3 = [\theta(L_{1,3}) - \pi, \theta(L_{0,1})]$, $\Phi_4 = [\theta(L_{0,1}), \theta(l(\bar{s}_1, \bar{z}(0,1,2)))]$, $\Phi_5 = [\theta(l(\bar{s}_1, \bar{z}(0,1,2))), \theta(l(\bar{s}_1, \bar{z}(1,2,3)))]$ and $\Phi_6 = [\theta(l(\bar{s}_1, \bar{z}(1,2,3))), \theta(L_{1,3}) + \pi]$. For the subregion Φ_3, the noise can have an arbitrary magnitude without making any decision error. On the other hand, for other regions Φ_4, Φ_5 and Φ_6, $d(\phi)$ can be determined as $\frac{d_{0,1}}{\cos(\pi/2 + \theta(L_{0,1}) - \phi)}$, $\frac{d_{1,2}}{\cos(\pi/2 + \theta(L_{1,2}) - \phi)}$ and $\frac{d_{1,3}}{\cos(\pi/2 + \theta(L_{1,3}) - \phi)}$, respectively. Moreover, we have $d_{1,3} = d_{0,2}$ and $\theta(L_{1,3}) = \theta(L_{0,2})$. Then, through some manipulations, the probability of correct decisions for $\bar{s}_1$ can be formulated as

$$\begin{aligned} &P_c(R, A|\bar{s}_1) \\ &= 1 - \xi(A, d_{0,1}, \theta(L_{0,1}), \Phi_4) - \xi(A, d_{0,2}, \theta(L_{0,2}), \Phi_6) \\ &\quad - \xi(A, d_{1,2}, \theta(L_{1,2}), \Phi_5). \end{aligned}$$

Since the symbols $\bar{s}_2$ and $\bar{s}_3$ are symmetric to $\bar{s}_1$ and $\bar{s}_0$ with respect to the origin, the decision regions for $\bar{s}_2$ and $\bar{s}_3$ are identical to those for $\bar{s}_1$ and $\bar{s}_0$, respectively. Using this symmetry, we can simply obtain the probability of correct decisions for each case as $P_c(R, A|\bar{s}_2) = P_c(R, A|\bar{s}_1)$ and $P_c(R, A|\bar{s}_3) = P_c(R, A|\bar{s}_0)$.

Finally, assuming that the transmitted symbols are equally likely, we can compute the overall probability of correct decisions $P_c(R, A)$ by combining the above probabilities. Then, the probability of error $P_e(R, A)$ can be obtained by $P_e(R, A) = 1 - P_c(R, A)$ as

$$\begin{aligned} P_e(R, A) &= \frac{1}{2}\xi(A, d_{0,1}, \theta(L_{0,1}), \Phi_0 \cup \Phi_4) \\ &+ \frac{1}{2}\xi(A, d_{0,2}, \theta(L_{0,2}), \Phi_2 \cup \Phi_6) \\ &+ \frac{1}{2}\xi(A, d_{1,2}, \theta(L_{1,2}), \Phi_5). \quad (7) \end{aligned}$$

In contrast, for the $R < 1$ case, the quadrature part is compressed by R. In other words, the inphase part is scaled up by $1/R$. From the inphase scaling point of view, the decision boundaries are formed by rotating the decision regions of Figure 2 by $\pi/2$. Thus, the final expression of the symbol error rate for $R < 1$ can be simply obtained from the $R > 1$ case by replacing R with $1/R$.

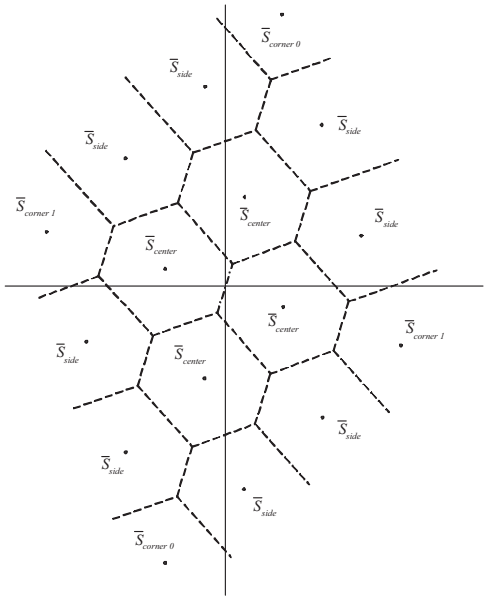

Fig. 3. New 16-QAM constellation $\bar{\mathcal{X}}$ and its decision region for $R > 1$.

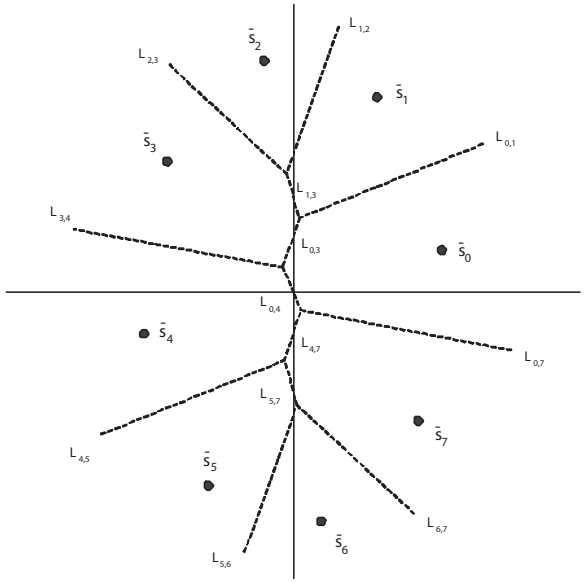

Fig. 4. New 8-PSK constellation $\bar{\mathcal{X}}$ and its decision region for $R > 1$.

Next we consider 16-QAM constellations. Figure 3 depicts the new constellation for 16-QAM and its decision boundaries when R is greater than 1. For the 16-QAM case, we can classify signal points into four groups: $\bar{S}_{corner0}$, $\bar{S}_{corner1}$, $\bar{S}_{side}$ and $\bar{S}_{center}$ according to the shape of its decision region. Here we use capital letters in order to distinguish from symbols of the 4-QAM constellation.

First we note that the probability of correct decisions for $\bar{S}_{corner0}$ and $\bar{S}_{corner1}$ are identical to that of $\bar{s}_0$ and $\bar{s}_1$ for 4-QAM constellations, respectively. Thus, we simply have $P_c(R, A|\bar{S}_{corner0}) = P_c(R, A|\bar{s}_0)$ and $P_c(R, A|\bar{S}_{corner1}) = P_c(R, A|\bar{s}_1)$.

For the case of $\bar{S}_{side}$ and $\bar{S}_{center}$, the decision regions are divided into four subregions and six subregions, respectively, which are listed in Table I. The detailed derivation is omitted to simplify the presentation. By substituting the parameters shown in Table I into (6), we can obtain $P_c(R, A|\bar{S}_{side})$ and $P_c(R, A|\bar{S}_{center})$ as

$$\begin{aligned} &P_c(R, A|\bar{S}_{side}) \\ &\quad = 1 - \xi(A, d_{0,1}, \theta(L_{0,1}), \Phi_0 \cup \Phi_4) \\ &\qquad -\xi(A, d_{0,2}, \theta(L_{0,2}), \Phi_7) - \xi(A, d_{1,2}, \theta(L_{1,2}), \Phi_5) \end{aligned}$$

and

$$\begin{aligned} &P_c(R, A|\bar{S}_{center}) \\ &\quad = 1 - 2\xi(A, d_{0,1}, \theta(L_{0,1}), \Phi_8) \\ &\qquad -2\xi(A, d_{0,2}, \theta(L_{0,2}), \Phi_7) - 2\xi(A, d_{1,2}, \theta(L_{1,2}), \Phi_5) \end{aligned}$$

where

$$\begin{aligned} \Phi_7 &= [\theta(l(\bar{s}_1, \bar{z}(1,2,3))), \theta(l(\bar{s}_0, \bar{z}(0,1,2))) + \pi] \\ \Phi_8 &= [\theta(l(\bar{s}_0, \bar{z}(0,1,2))), \theta(l(\bar{s}_1, \bar{z}(0,1,2)))]. \end{aligned}$$

Therefore, using above probabilities of the correct decision for each constellation point, the probability of error for 16-QAM given A and R is expressed as

$$\begin{aligned} &P_e(R, A) \\ &= 1 - \frac{1}{16}\Big\{2P_c(R, A|\bar{S}_{corner0}) + 2P_c(R, A|\bar{S}_{corner1}) \\ &\qquad + 8P_c(R, A|\bar{S}_{side}) + 4P_c(R, A|\bar{S}_{center}))\Big\} \\ &= \frac{5}{8}\xi(A, d_{0,1}, \theta(L_{0,1}), \Phi_0 \cup \Phi_4) + \frac{1}{2}\xi(A, d_{0,1}, \theta(L_{0,1}), \Phi_8) \\ &\quad + \frac{1}{8}\xi(A, d_{0,2}, \theta(L_{0,2}), \Phi_2 \cup \Phi_6) + \frac{1}{2}\xi(A, d_{0,2}, \theta(L_{0,2}), \Phi_7) \\ &\quad + \frac{9}{8}\xi(A, d_{1,2}, \theta(L_{1,2}), \Phi_8). \end{aligned} \tag{8}$$

B. Error Rates for 8-PSK Constellation

In Figure 4, we depict the new 8-PSK constellation and its decision boundaries. Using the same manner as in the M-QAM constellation case, we can obtain the probability of correct decision for $\bar{s}_k$ $(k = 0, 1, 2, 3)$ given R and A as

$$\begin{aligned} &P_c(R, A|\bar{s}_0) \\ &\quad = 1 - \xi(A, d_{0,1}, \theta(L_{0,1}), \Theta_1) - \xi(A, d_{0,3}, \theta(L_{0,3}), \Theta_2) \\ &\qquad - \xi(A, d_{0,4}, \theta(L_{0,4}), \Theta_3) - \xi(A, d_{0,7}, \theta(L_{0,7}), \Theta_4), \end{aligned} \tag{9}$$

$$\begin{aligned} &P_c(R, A|\bar{s}_1) \\ &\quad = 1 - \xi(A, d_{1,2}, \theta(L_{1,2}), \Theta_5) - \xi(A, d_{1,3}, \theta(L_{1,3}), \Theta_6) \\ &\qquad - \xi(A, d_{0,1}, \theta(L_{0,1}), \Theta_7), \end{aligned} \tag{10}$$

$$\begin{aligned} &P_c(R, A|\bar{s}_2) \\ &\quad = 1 - \xi(A, d_{2,3}, \theta(L_{2,3}), \Theta_8) - \xi(A, d_{1,2}, \theta(L_{1,2}), \Theta_9), \end{aligned} \tag{11}$$

and

$$\begin{aligned} &P_c(R, A|\bar{s}_3) \\ &\quad = 1 - \xi(A, d_{1,3}, \theta(L_{1,3}), \Theta_{10}) - \xi(A, d_{2,3}, \theta(L_{2,3}), \Theta_{11}) \\ &\quad -\xi(A, d_{3,4}, \theta(L_{3,4}), \Theta_{12}) - \xi(A, d_{0,4}, \theta(L_{0,4}), \Theta_{13}) \end{aligned} \tag{12}$$

where Θ_i's indicate subregions for each constellation point listed in Table II. Moreover, the probability of correct decision

TABLE I
PARAMETERS FOR $\bar{S}_{side}$ AND $\bar{S}_{center}$ IN 16-QAM

$\bar{S}_{side}$	angle	$[\theta_3-\pi, \theta_1]$	$[\theta_1, \theta_4]$	$[\theta_4, \theta_5]$	$[\theta_5, \theta_3+\pi]$	-	-
	$d(\phi)$	$\frac{d_{0,1}}{\cos(\pi/2-\theta_1+\phi)}$	$\frac{d_{0,1}}{\cos(\pi/2+\theta_1-\phi)}$	$\frac{d_{1,2}}{\cos(\pi/2+\theta_6-\phi)}$	$\frac{d_{0,2}}{\cos(\pi/2+\theta_2-\phi)}$	-	-
$\bar{S}_{center}$	angle	$[\theta_5, \theta_3+\pi]-\pi$	$[\theta_3, \theta_4]$	$[\theta_4, \theta_5]$	$[\theta_5, \theta_3+\pi]$	$[\theta_3, \theta_4]+\pi$	$[\theta_4, \theta_5]+\pi$
	$d(\phi)$	$\frac{d_{0,2}}{\cos(\pi/2-\theta_2+\phi)}$	$\frac{d_{0,1}}{\cos(\pi/2+\theta_1-\phi)}$	$\frac{d_{1,2}}{\cos(\pi/2+\theta_6-\phi)}$	$\frac{d_{0,2}}{\cos(\pi/2+\theta_2-\phi)}$	$\frac{d_{0,1}}{\cos(\pi/2-\theta_1+\phi)}$	$\frac{d_{1,2}}{\cos(\pi/2-\theta_6+\phi)}$
$\theta_1=\theta(L_{0,1})$, $\theta_2=\theta(L_{0,2})$, $\theta_3=\theta(l(\bar{s}_0,\bar{z}(0,1,2)))$, $\theta_4=\theta(l(\bar{s}_1,\bar{z}(0,1,2)))$, $\theta_5=\theta(l(\bar{s}_1,\bar{z}(1,2,3)))$, $\theta_6=\theta(L_{1,2})$							

TABLE II
SUBREGIONS FOR $\bar{s}_0$, $\bar{s}_1$, $\bar{s}_2$ AND $\bar{s}_3$ IN 8-PSK CONSTELLATION

Symbol	Subregions	Angle
$\bar{s}_0$	Θ_1	$[\theta(L_{0,1}), \theta(l(\bar{s}_0, \bar{z}(0,1,3)))]$
	Θ_2	$[\theta(l(\bar{s}_0, \bar{z}(0,1,3))), \theta(l(\bar{s}_0, \bar{z}(0,3,4)))]$
	Θ_3	$[\theta(l(\bar{s}_0, \bar{z}(0,3,4))), \theta(l(\bar{s}_0, \bar{z}(0,4,7))) + \pi]$
	Θ_4	$[\theta(l(\bar{s}_0, \bar{z}(0,3,7))), \theta(L_{0,7})] + \pi$
$\bar{s}_1$	Θ_5	$[\theta(L_{1,2}), \theta(l(\bar{s}_1, \bar{z}(1,2,3))) + \pi]$
	Θ_6	$[\theta(l(\bar{s}_1, \bar{z}(1,2,3))), \theta(l(\bar{s}_1, \bar{z}(0,1,3)))] + \pi$
	Θ_7	$[\theta(l(\bar{s}_1, \bar{z}(0,1,3))) - \pi, \theta(L_{0,1})]$
$\bar{s}_2$	Θ_8	$[\theta(l(\bar{s}_2, \bar{z}(1,2,3))) - \pi, \theta(L_{1,2})]$
	Θ_9	$[\theta(L_{2,3}), \theta(l(\bar{s}_1, \bar{z}(1,2,3))) + \pi]$
$\bar{s}_3$	Θ_{10}	$[\theta(l(\bar{s}_3, \bar{z}(0,1,3))) - \pi, \theta(l(\bar{s}_3, \bar{z}(1,2,3)))]$
	Θ_{11}	$[\theta(l(\bar{s}_3, \bar{z}(1,2,3))), \theta(L_{2,3})]$
	Θ_{12}	$[\theta(L_{3,4}), \theta(l(\bar{s}_3, \bar{z}(0,3,4))) + \pi]$
	Θ_{13}	$[\theta(l(\bar{s}_3, \bar{z}(0,3,4))), \theta(l(\bar{s}_3, \bar{z}(0,1,3)))] + \pi$

for the rest of symbols can easily be computed using the symmetry of decision regions as $P_c(R, A|\bar{s}_k) = P_c(R, A|\bar{s}_{k-4})$ for $k = 4, 5, 6$ and 7. Therefore, the error probability for 8-PSK constellation given R and A can be computed as

$$P_e(R, A) = 1 - \frac{1}{4}\sum_{k=0}^{3} P_c(R, A|\bar{s}_k) \tag{13}$$

where $P_c(R, A|\bar{s}_k)$'s are obtained from (9) - (12).

C. Joint PDF of R and A

In order to compute the probability of error, we need to average the error probability $P_e(R, A)$ with respect to the noise variance A and the ratio R, as these two random variables are determined by the channel condition.

For computing the joint pdf of A and R, we first consider the conditional cumulative density function (cdf) of R given $A = \alpha$, which is defined as $F_R(r|\alpha) = \Pr\{R < r \mid A = \alpha\}$. From the definitions $R = \sigma_I/\sigma_Q = |h[m]|/|h[n]|$ and $A = N_0/2|h[n]|^2$, the conditional cdf of R can be expressed as

$$\begin{aligned} F_R(r|\alpha) &= \Pr\left\{\frac{|h[m]|}{|h[n]|} < r \;\middle|\; \frac{N_0}{2|h[n]|^2} = \alpha\right\} \\ &= \Pr\left\{|h[m]| < r|h[n]| \;\middle|\; |h[n]|^2 = \frac{N_0}{2\alpha}\right\} \\ &= \Pr\left\{|h[m]| < r\sqrt{\frac{N_0}{2\alpha}}\right\} \\ &= \int_0^{r\sqrt{\frac{N_0}{2\alpha}}} f_h(x)dx \\ &= F_h\left(r\sqrt{\frac{N_0}{2\alpha}}\right) - F_h(0) \end{aligned} \tag{14}$$

where $f_h(\cdot)$ and $F_h(\cdot)$ indicate the pdf and the cdf of $|h[m]|$, respectively.

In this letter, we consider the Rician fading channel with the Rician factor $K = \Gamma^2/2\sigma^2$ where Γ^2 and $2\sigma^2$ stand for the power of the specular component and the diffuse component, respectively. Then, the Rician pdf is expressed as

$$f_h(x) = \frac{x}{\sigma^2}\exp\left(-\frac{x^2+\Gamma^2}{2\sigma^2}\right) I_0\left(\frac{x\Gamma}{\sigma^2}\right)$$

where $I_0(\cdot)$ is the modified Bessel function of the first kind and zero order. By differentiating the cdf (14) with respect to r, we can compute the conditional pdf of R given $A = \alpha$ as

$$f_R(r|\alpha) = \frac{rN_0}{2\alpha\sigma^2}\exp\left(-\frac{r^2N_0 + 2\alpha\Gamma^2}{4\alpha\sigma^2}\right) I_0\left(\frac{r\Gamma}{\sigma^2}\sqrt{\frac{N_0}{2\alpha}}\right).$$

Also, the marginal pdf of A is obtained directly by a change of variables according to the relation between A and the magnitude of the channel as

$$f_A(\alpha) = \frac{N_0}{4\alpha^2\sigma^2}\exp\left(-\frac{N_0 + 2\alpha\Gamma^2}{4\alpha\sigma^2}\right) I_0\left(\frac{\Gamma}{\sigma^2}\sqrt{\frac{N_0}{2\alpha}}\right).$$

Using the above two expressions and Bayes' theorem, the joint pdf of R and A can be expressed as

$$\begin{aligned} f_{R,A}(r, \alpha) &= f_R(r|\alpha) f_A(\alpha) \\ &= \frac{rN_0^2}{8\alpha^3\sigma^4}\exp\left(-\frac{(r^2+1)N_0 + 4\alpha\Gamma^2}{4\alpha\sigma^2}\right) \\ &\quad \times I_0\left(\frac{r\Gamma}{\sigma^2}\sqrt{\frac{N_0}{2\alpha}}\right) I_0\left(\frac{\Gamma}{\sigma^2}\sqrt{\frac{N_0}{2\alpha}}\right). \end{aligned} \tag{15}$$

Finally, utilizing the results of $P_e(R, A)$ in (7), (8), (13) and $f_{R,A}(r, \alpha)$ in (15), we can get the average SER for Rician channels by integrating the conditional error rates over ranges of R and A as

$$P_e = \int_0^\infty \int_0^\infty P_e(r, \alpha) f_{R,A}(r, \alpha) dr d\alpha.$$

Note that the above integral is evaluated numerically.

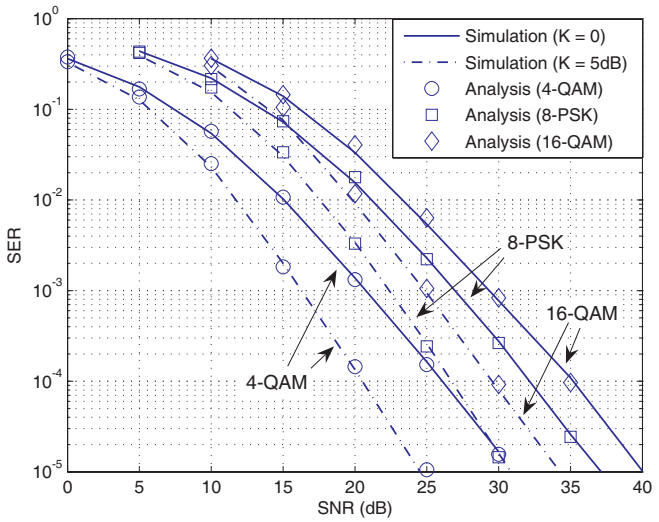

Fig. 5. SER comparison of numerical results and the analysis.

IV. Simulation Results

In this section, we show simulation results to verify the accuracy of our analysis derived in the previous section. Figure 5 depicts the average SER for 4-QAM, 8-PSK and 16-QAM over Rician channels with various values of K versus the average received SNR. Here, the average received SNR is E_s/N_0 where E_s indicates the average symbol energy. In our simulation, we choose $\theta_R = \pi/8$ radians as the rotation angle for both 4-QAM and 16-QAM constellations and $\theta_R = 0.15$ radian for 8-PSK as suggested in [2] [13]. In this figure, we plot our analysis results as the solid line and the computer simulations as the circle point. It is clear from these simulation results that our analysis is accurate compared to the actual simulation. Since our analysis method is applicable for the SSD scheme with any rotation angle θ_R, this can be used to verify the performance of systems with various rotating angles.

V. Conclusions

In this letter, we have derived an exact SER expression for the SSD in fading channels based on the new signal model. For our analysis, we have used polar coordinates instead of rectangular coordinates to derive the exact error probability for the case of asymmetric decision regions. By applying the distributions of the magnitude and the phase of the noise in the polar coordinate, we can accurately compute the probability of error in Rician fadings. From simulations, we have confirmed the accuracy of our analysis for 4-QAM,16-QAM and 8-PSK.

VI. Acknowledgment

The authors would like to thank Prof. Alouini and the reviewers for helpful remarks.

References

[1] V. Tarokh, N. Seshadri, and A. R. Calderbank, "Space-Time codes for high data rate wireless communication: performance criterion and code construction," *IEEE Trans. Inform. Theory*, vol. IT-44, pp. 744-765, Mar. 1998.

[2] J. Boutros and E. Viterbo, "Signal space diversity: a power- and bandwidth-efficient diversity technique for the Rayleigh fading channel," *IEEE Trans. Inform. Theory*, vol. 44, pp. 1453-1467, July 1998.

[3] M. K. Simon and M.-S. Alouini, "A unified approach to the performance analysis of digital communication over generalized fading channels," *Proc. IEEE*, vol. 86, pp. 1860-1877, Sept. 1998.

[4] X. Dong, N. C. Beaulieu, and P. H. Wittke, "Signaling constellations for fading channels," *IEEE Trans. Commun.*, vol. 47, pp. 703-714, May 1999.

[5] G. Taricco and E. Viterbo, "Performance of component interleaved signal sets for fading channels," *IEE Electron. Lett.*, vol. 32, pp. 1170-1172, June 1996.

[6] G. Taricco and E. Viterbo, "Performance of high-diversity multidimensional constellations," *IEEE Trans. Inform. Theory*, vol. 44, pp. 1539-1543, July 1998.

[7] J.-C. Belfiore and E. Viterbo, "Approximating the error probability for the independent Rayleigh fading channel," in *Proc. International Symp. Inform. Theory*, p. 362, Sept. 2005.

[8] A. G. I. Fabregas and E. Viterbo, "Sphere lower bound for rotated lattice constellations in fading channels," *IEEE Trans. Wireless Commun.*, vol. 7, pp. 825-830, Mar. 2008.

[9] R. F. Pawula, S. O. Rice, and J. H. Roberts, "Distribution of the phase angle between two vectors perturbed by Gaussian noise," *IEEE Trans. Comunn.*, vol. 30, pp. 1828-1841, Aug. 1982.

[10] F. S. Weinstein, "Simplified relationships for the probability distribution of the phase of a sine wave in narrow-band normal noise," *IEEE Trans. Inform. Theory*, vol. IT-20, pp. 658-661, Sept. 1974.

[11] L. Szczecinski, S. Aissa, C. Gonzalez, and M. Bacic, "Exact evaluation of bit- and symbol error rates for arbitrary two-dimensional modulation and non-uniform signaling in AWGN channel," *IEEE Trans. Commun.*, vol. 54, pp. 1049-1056, June 2006.

[12] J. M. Cioffi, 379A class note: signal processing and detection, Stanford Univ.

[13] A. Chindapol and J. A. Ritcey, "Bit-interleaved coded modulation with signal space diversity in Rayleigh fading," in *Proc. 33rd Asilomar Conf. Signals, Systems Computers*, pp. 1003-1007, Oct. 1999.